Hardware-in-the-Loop pantograph tests with general overhead contact line geometry

M. Tur[a,*], S. Gregori[a], A. Correcher[b], J. Gil[a], A. Pedrosa[a], F.J. Fuenmayor[a]

[a] *Instituto de Ingeniería Mecánica y Biomecánica, Universitat Politècnica de València, 46022, Valencia, Spain*
[b] *Instituto de Automática e Informática Industrial, Universitat Politècnica de València, 46022, Valencia, Spain*

Abstract

Hardware-in-the-loop testing serves as a method to examine the dynamic interaction between the pantograph and catenary within controlled laboratory environments. This task involves measuring the force from the pantograph, using a real-time catenary model to determine the next pantograph position, and generating the desired pantograph movement to complete the loop. To address potential instability issues arising from communication delays and the inherent stiffness in the interaction with pantograph strips, a mass-spring system and a Linear Quadratic Gaussian controller are integrated into the system. The catenary is a finite element model of a complete section, incorporating the non-linearity introduced by dropper slackening. Validation of the results demonstrates a good level of accuracy in the HiL test approach within the frequency range of 0-20 Hz.

Keywords: LQG controller ; Pantograph-catenary ; Hardware-in-the-loop ; Hybrid simulation

---

1. Introduction

Hardware-in-the-loop (HiL) testing [1, 2, 3] is a method of assessing the performance and reliability of mechatronic systems. HiL testing integrate physical hardware components into a simulated environment, to enable engineers to evaluate the system‘s behaviour in real-world conditions. Hybrid Simulation (HS) [4, 5, 6] is a broader testing approach that combines physical and computational elements to evaluate the behaviour of an entire system or structure in which only a part of the system is physically tested, while the rest is simulated in a computational environment. The physical and virtual components are connected in real time, allowing interactions between them. HS faces specific challenges related to the stability of the systems due to delays in the signals, delays on the actuators, or high-frequency components included in the computation phase [7, 8]. Although there are differences, in the context of pantograph-catenary system the terms HS or HiL have been interchangeably used in the literature to describe tests involving a real pantograph interacting with an actuator behaving in accordance with a numerical catenary model. Throughout this work the term HiL is used.

Computer simulation is a powerful modeling tool commonly used in designing new overhead contact lines (also known as catenaries) for railways and assessing interaction with the pantograph. EN50318 regulation describes the requirements for validation of numerical simulation codes. The overhead contact line (OCL) computational model should contain the main components of the structure, such as contact and catenary wires, droppers and steady arms, and should fulfill the geometry and conditions imposed in the OCL assembly. The pantograph is usually simulated as a lumped mass model in which only the vertical dynamics is considered. The state-of-the-art in simulation models can be found in [20]. EN50318 standard allows the use of real pantographs to assess the interaction with an OCL computational model, this being the first application of HiL tests. In addition, HiL can be used to test new pantographs or new components, such as contact strips or suspensions, guaranteeing the safety and reliability of the system. It can also be used to improve current collection quality developing active pantograph systems through the interaction with a catenary model.

Testing of pantographs is essential to guarantee the safety, reliability, and economic sustainability of railway systems. In this work we propose a HiL method for testing the pantograph-catenary interaction. This is a complex task that requires measuring the force from the real pantograph, and putting the measure into a real-time catenary model that computes the next pantograph position, and generate the desired movement of the pantograph, thus closing the loop. Some factors can generate complexity in the problem: non-linearities, non-modeled dynamics on Pantographs, delays on the actuator, delays on the force measures, noise in the force measure, or high frequencies generated in the system, among others.

The literature contains various approaches to HS or HiL testing, using different catenary models with varying degrees of approximation and diverse actuation and control technologies.

---

[*] Corresponding author

Email addresses: `manuel.tur@mcm.upv.es` (M. Tur), `sangreve@upv.es` (S. Gregori), `ancorsal@ai2.upv.es` (A. Correcher), `jaigiro@upv.es` (J. Gil), `anpedsan@upv.es` (A. Pedrosa), `ffuenmay@mcm.upv.es` (F.J. Fuenmayor)

Preprint submitted to Mechatronics *November 6, 2024*

In 2002, a test rig was developed for the hybrid simulation of pantograph-catenary system [9]. The catenary model consists of five equal spans. Contact and support wires were modeled using a modal basis and droppers as linear springs. This model was solved in real time with a time increment of 2 ms using a PII computer with 300 MHz processor.

In Politecnico di Milano (see [10] and references therein) the test rig includes an electrohydraulic actuator for the vertical movement and an electric motor for the lateral movement (stagger of the catenary). The real-time catenary model is composed of two tensioned wires joined by non-linear droppers and the motion of the system is represented by a reduced number of d.o.f. and sinusoidal functions in both the messenger and the contact wire. This catenary has a length of 3 or 5 spans and a shift-forward strategy allows the emulation of a longer catenary. The frequency range of validity is 0-20 Hz. In their last published work [10], HiL test results with the ATR95 pantograph and C270 Italian catenary were presented.

In TUW, Schirrer et al. [11] proposed more complex catenary model characterised by the use of moving coordinates, finite differences and absorbing boundary layers to dissipate outgoing perturbations. It is also intended for the 0-20 Hz range, although the actuator is formed by an industrial robot and a linear motor, thus allowing higher speeds and broader bandwidths. This approach includes a Model Predictive Control (MPC) to guarantee stability in the HiL tests despite the test rig limitations, uncertainty in the pantograph model, and measurement noise.

The work of Kobayashi et al. [12] shows the latest tests performed at RTRI in Tokyo where a lumped mass system with multiple degrees of freedom is used to simulate the catenary. The test rig includes a servohydraulic actuator to impose vertical displacement on the pantograph. The paper shows that several issues, such as modelling errors, significantly affect the simulation accuracy, so they must include a controller to guarantee realistic testing. In this case, a substructure control algorithm is included in parallel with the pantograph-catenary interaction loop to ensure that the pantograph moves according to the simulated catenary contact point. The HiL experimental results are compared with a fully simulated HiL test, showing better agreement in the frequency domain than in time domain.

In previous works, the authors performed HiL tests with two different catenary models. The first one [13] is a broad simplification in which a tensioned string and viscoelastic layer emulate the dynamic behaviour of the catenary. The second catenary model [14] is a faithful finite element model with non-linear droppers which allows only periodic pantograph-catenary interaction. In those works a delay compensation technique was employed, leading to accurate results in the 0-25 Hz range. Note that all the works found in the literature consider a periodic arrangement of the catenary in their HiL tests.

The aim of this paper is to propose a new algorithm for HiL pantograph testing using a Linear Quadratic Gaussian (LQG) controller. The catenary is a finite element model of a complete section that can be solved in real time and is based on modal decomposition and offline precomputation of certain matrices. It considers non-linear dropper slackening and general geometry including different number of droppers per span, contact height, etc. The test rig system is split into two subsystems for the HiL algorithm. The first is the real-time catenary model that includes an intermediate interaction mass-spring system between the measured force and the numerical model. The second subsystem is composed of the measurement and communication devices, actuator and pantograph. An LQG controller is proposed for the second subsystem with the objective of minimizing the difference between the reference position sent to the actuator and its real position.

The paper is organized as follows: Section 2 describes the catenary model. The real-time model is assessed by comparing the results with a catenary simulation code validated according to EN50318 [15]. Section 3 describes the HiL test rig components and operation. The main contribution of the paper can be found in Section 4, in which a the LQG controller is proposed for the HiL actuator consists of a state space Linear Quadratic Regulator (LQR) plus a Kalman Filter (KF) for state estimation. The results of the HiL test and validation of the proposed method are given in Section 5. The paper finalizes with the conclusions.

2. Real-time catenary model

HiL testing requires the catenary model to be solved in real-time, i.e. given a contact force, the model must provide the position of the pantograph contact point faster than the integration scheme time step. A high time increment allows adding more degrees of freedom and features to the catenary model but has the disadvantage of reducing simulation accuracy. A time increment of $\Delta t = 2\,\mathrm{ms}$ provides a good balance between accuracy and real-time capabilities, as analysed in [16]. Here, we follow the method presented in the previously cited work to develop the real-time catenary model. For the sake of clarity, we recall here its main features but refer readers to [17] for further details of the formulation. In Section 2.3, we extend the model to solve the interaction between the pantograph and the catenary through an intermediate system.

The finite element code of the catenary, proposed in [18] for the static and [19] for the dynamic problem, is taken as a reference for comparison with the real-time model simulations (see Section 2.4). This code was validated in the catenary Benchmark [20] and according to EN50318 [15].

Figure 1 shows a scheme of the finite element model of an OCL with 20 spans each of $L = 65\,\mathrm{m}$ length. Note that the image is distorted due to different scales of the horizontal and vertical axes. The structural elements that support the whole system (masts and cantilevers) are replaced by equivalent boundary conditions. The contact

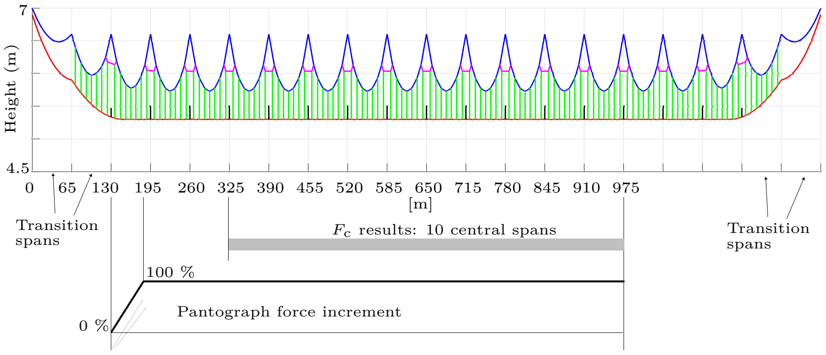

Figure 1: Finite element model of a 20-span catenary section. Pantograph force is gradually introduced from span 3.

wire (shown in red) interacts with the pantograph located on the vehicle's roof, and is held at a predefined height with the help of droppers (shown in green), steady arms (shown in black) and the carrier wire (shown in blue). The carrier wire and steady arms are supported regularly on brackets (not shown) at a certain height over the track. The droppers are fixed to the contact and carrier wires by clamps. The stitch wire (shown in purple) modifies the stiffness of the catenary near the supports. As in the case of the droppers, clamps are used to attach the stitch wires to the carrier and contact wires.

A general catenary geometry can be simulated. The first and last two spans are transition spans with wire elevation, while every internal spans can have a different number of droppers and mast distance. Contact and messenger wires are discretized with ANCF elements, whilst droppers and steady arms are modeled by articulated bar elements. Wire tractions and the conditions imposed in the catenary stringing are also considered (see [18] for details). The pantograph interaction is gradually introduced from span number 3, with a 50 m ramp in which the pantograph force is linearly increased.

2.1. Dynamic simulation of a single section

The static configuration problem is solved using the non-linear full finite element model of a single section [18]. The problem is linearized in that configuration and some matrices and vectors are extracted for use in the real-time dynamic model:

- Mass matrix $\mathbf{M}_{\mathrm{c}}$, damping matrix $\mathbf{C}_{\mathrm{c}}$ and stiffness matrix $\mathbf{K}_{\mathrm{c}}$. The dimension of these squared matrices is the number of degrees of freedom of the discretization, n_{dof}. Proportional damping is considered.
- $\mathbf{z}_{\mathrm{c}}^{0}$: Vector of dimension n_{dof} containing the static position nodal degrees of freedom.
- $\mathbf{F}_{\mathrm{d}}^{0}$: Vector containing the traction forces exerted by the n_{d} droppers in the static configuration.

In addition to the above, some other matrices are precomputed for convenience in an offline stage, to achieve real-time capabilities. We assume a constant train speed V and a single contact point, so that the pantograph position is known in advance and the n_{c} potential contact points on the contact wire can be obtained. Each contact point is associated with a time step t. $\mathbf{N}_{\mathrm{c}}^{t}$ denotes the interpolation vector, which extracts the contact point magnitude at time t from the total nodal values. Subindex c in this vector refers to the catenary's degrees of freedom involved in the interpolation. This operator also allows the contact force to be transfered to the finite element nodes every time step.

Using the matrices defined above, the dynamic equilibrium problem at time t can be written as :

$$\mathbf{M}_{\mathrm{c}}\ddot{\mathbf{u}}_{\mathrm{c}}^{t} + \mathbf{C}_{\mathrm{c}}\dot{\mathbf{u}}_{\mathrm{c}}^{t} + \mathbf{K}_{\mathrm{c}}\mathbf{u}_{\mathrm{c}}^{t} = {\mathbf{N}_{\mathrm{c}}^{t}}^{\mathrm{T}} F_{\mathrm{c}}^{t-1} \qquad t = 1, \ldots, n_{\mathrm{c}} \tag{1}$$

where $\mathbf{u}_{\mathrm{c}}^{t}$, $\dot{\mathbf{u}}_{\mathrm{c}}^{t}$ and $\ddot{\mathbf{u}}_{\mathrm{c}}^{t}$, are displacement, velocity and acceleration nodal vectors at time t, respectively. It should be noted that the contact force measured at time t, F_{c}^{t} is not available due to the communication delays in a HiL test, so that the value measured in the previous time step F_{c}^{t-1} is used as the external force (see Section 3).

This problem can be expressed on a modal basis by solving the generalized eigenvalue problem. If $\mathbf{\Phi}$ denotes the eigenvector matrix, the transformation between nodal displacement and the modal basis can be written as:

$$\mathbf{u}_{\mathrm{c}}^{t} = \mathbf{\Phi}\,\mathbf{q}_{\mathrm{c}}^{t} \tag{2}$$

where $\mathbf{q}_{\mathrm{c}}^{t}$ is the vector of modal coordinates defining the position at time t. The same transformation applies to velocity and acceleration. Matrix $\mathbf{\Phi}$ dimension is $n_{\mathrm{dof}} \times n_{\mathrm{mod}}$, n_{mod} being the number of modes. This number can be chosen as detailed in [17] to obtain accurate solutions (compared with the complete solution) at a lower computational cost.

Eq. (1) is solved using the Newmark integration scheme (see [16] for details). Given the position, velocity and acceleration at time $t-1$, and assuming that the external force F_{c}^{t-1} is known, the solution at time t can be written as:

$$\mathbf{K_{it}}_{\mathrm{c}}\mathbf{u}_{\mathrm{c}}^{t} = \mathbf{m_U}\mathbf{u}_{\mathrm{c}}^{t-1} + \mathbf{m_V}\dot{\mathbf{u}}_{\mathrm{c}}^{t-1} + \mathbf{m_A}\ddot{\mathbf{u}}_{\mathrm{c}}^{t-1} + {\mathbf{N}_{\mathrm{c}}^{t}}^{T} F_{\mathrm{c}}^{t-1} \tag{3}$$

where $\mathbf{K_{it}}_{\mathrm{c}}$, $\mathbf{m_U}$, $\mathbf{m_V}$ and $\mathbf{m_A}$ are constant matrices depending on the integration scheme parameters and mass, damping and stiffness matrices (see Appendix A). Once the position is obtained, the velocity and acceleration at time t can be recovered. Eq. (3) can be projected in the modal basis as:

$$\begin{aligned} \widehat{\mathbf{K}}_{\mathbf{itc}} \mathbf{q}_{\mathrm{c}}^{t} =& \widehat{\mathbf{m}}_{\mathbf{U}} \mathbf{q}_{\mathrm{c}}^{t-1} + \widehat{\mathbf{m}}_{\mathbf{V}} \dot{\mathbf{q}}_{\mathrm{c}}^{t-1} + \widehat{\mathbf{m}}_{\mathbf{A}} \ddot{\mathbf{q}}_{\mathrm{c}}^{t-1} + \widehat{\mathbf{N}}_{\mathrm{c}}^{t\ \mathrm{T}} F_{\mathrm{c}}^{t-1} \\ & \widehat{\mathbf{K}}_{\mathbf{itc}} = \mathbf{\Phi}^{\mathrm{T}} \mathbf{K_{it}}_{\mathrm{c}} \mathbf{\Phi} \\ & \widehat{\mathbf{m}}_{\mathbf{U}} = \mathbf{\Phi}^{\mathrm{T}} \mathbf{m_U} \mathbf{\Phi} \qquad \widehat{\mathbf{m}}_{\mathbf{V}} = \mathbf{\Phi}^{\mathrm{T}} \mathbf{m_V} \mathbf{\Phi} \\ & \widehat{\mathbf{m}}_{\mathbf{A}} = \mathbf{\Phi}^{\mathrm{T}} \mathbf{m_A} \mathbf{\Phi} \qquad \widehat{\mathbf{N}}_{\mathrm{c}}^{t} = \mathbf{\Phi}^{\mathrm{T}} \mathbf{N}_{\mathrm{c}}^{t} \end{aligned} \tag{4}$$

Given that a proportional damping model is used, the projected matrices are diagonal, and can be precomputed in an offline stage. The computational cost is reduced to multiplying and adding vectors of dimension n_{mod}. All this allows Eq. (4) to be evaluated much faster than real-time.

It is convenient to define the space state vector of the catenary using displacement, velocity and acceleration as:

$$\mathbf{x}_{\mathrm{c}} = \left\{ \begin{array}{c} \mathbf{q}_{\mathrm{c}} \\ \dot{\mathbf{q}}_{\mathrm{c}} \\ \ddot{\mathbf{q}}_{\mathrm{c}} \end{array} \right\} \tag{5}$$

Using the above definition, Eq. (4) can be written in state space form as:

$$\mathbf{x}_{\mathrm{c}}^{t} = \mathbf{A}_{\mathrm{c}} \, \mathbf{x}_{\mathrm{c}}^{t-1} + \mathbf{B}_{\mathrm{c}} \, F_{\mathrm{c}}^{t-1} \tag{6}$$

where the matrices are defined in Appendix A. It should be noted that every block in $\mathbf{A}_{\mathrm{c}}$ and $\mathbf{B}_{\mathrm{c}}$ is a diagonal matrix.

The contact point height at time t, z_{c}^{t}, is computed from the modal solution and static configuration as:

$$z_{\mathrm{c}}^{t} = \mathbf{N}_{\mathrm{c}}^{t} \, \mathbf{z}_{\mathrm{c}}^{0} + \widehat{\mathbf{N}}_{\mathrm{c}}^{t} \, \mathbf{q}_{\mathrm{c}}^{t} \tag{7}$$

2.2. Dropper slackening

Eq. (3) (or Eq. (4) in modal coordinates) gives the nodal displacements at time t assuming a linear behavior of the catenary. However, the droppers behave non-linearly as they can only transmit traction loads, i.e. the compressive load transmitted by each dropper j due to dynamic displacements, should be lower than the static traction. If $\mathbf{F}_{\mathrm{d}}^{0}$ is the vector of dimension n_{d} containing the static traction of each dropper, this condition can be expressed as:

$$\left(\mathbf{F}_{\mathrm{d}}^{0}\right)_{j} + \left(\mathbf{I}_{\mathrm{dc}} \, \mathbf{q}_{\mathrm{c}}^{t}\right)_{j} \geq 0 \qquad j = 1, \ldots, n_{\mathrm{d}} \tag{8}$$

where $\mathbf{I}_{\mathrm{dc}}$ is a full matrix, with dimensions $n_{\mathrm{d}} \times n_{\mathrm{mod}}$, that condenses the influence of modal degrees of freedom (computed from Eq. (4)) on the traction force generated in each dropper, precomputed in the offline stage (see [16] for details). Operator $(\cdot)_j$ extracts the j-th component of the vector. This equation must be verified every time step.

Should Eq. (8) fail for a given dropper j, a traction correction force vector $\mathbf{F}_{\mathrm{d}}^{t}$ is computed for that time step t. This is nonzero only in the rows of slackened droppers, and is applied as an external force to the catenary model. Using the time integration solver offline, we can obtain the effect of each dropper force in the nodal displacement. In addition, a change in displacements affects the dropper force. This influence, i.e. the effect of a unit dropper external force in the traction of other droppers, can be condensed in the matrix $\mathbf{I}_{\mathrm{dd}}$ with dimension $n_{\mathrm{d}} \times n_{\mathrm{d}}$, which can be computed offline. The correction force is thus obtained by solving a system of equations of the order of the number of slackened droppers:

$$\begin{gathered} \left(\mathbf{F}_{\mathrm{d}}^{0}\right)_{j} + \left(\mathbf{I}_{\mathrm{dc}} \, \mathbf{q}_{\mathrm{c}}^{t}\right)_{j} + \left(\mathbf{F}_{\mathrm{d}}^{t}\right)_{j} + \left(\mathbf{I}_{\mathrm{dd}} \, \mathbf{F}_{\mathrm{d}}^{t}\right)_{j} = 0 \\ \text{for} \quad j \in \text{slackened droppers} \end{gathered} \tag{9}$$

2.3. Interaction with pantograph

The penalty method is a technique commonly used in simulation codes to solve the contact interaction between a numerical pantograph model and the catenary contact wire [20]. In this method, a contact stiffness k_{c} is introduced between the moving catenary contact point (height z_{c}) and the degree of freedom of the pantograph head model u_{p} (usually the upper mass of a lumped mass model). The contact force is computed as:

$$F_{\mathrm{c}}^{t} = k_{\mathrm{c}} \left(z_{\mathrm{c}}^{t} - u_{\mathrm{p}}^{t} \right) \tag{10}$$

The contact stiffness k_{c} is a user-defined parameter. A low k_{c} value results in a large error of the contact constraint, causing the position of the pantograph head to differ from that of the catenary. On the other hand, excessive contact stiffness leads to numerical instabilities in the integration scheme. The problem is exacerbated if an explicit solver is used, because the catenary and pantograph dynamics are computed independently with a delay: the contact wire position z_{c}^{t} is obtained by solving the catenary dynamics with the contact force of the previous time step (F_{c}^{t-1}, Eq. (3)). This position is imposed in the upper mass of the pantograph through the contact spring k_{c}, to obtain u_{p}^{t} and the next applied contact force with Eq. (10). In general, stiffness values higher than 100.000 N/m make the explicit method unstable (see [14] for example). In the regulation EN50318 this parameter is set to 50.000 N/m.

In a HiL context, the pantograph model is replaced by the real contact force, and this force is applied to the catenary with a delay of at least one time step, similar to an explicit solver. This contact force is measured as the interaction between the load cell contact pad and the pantograph strips. This interaction can be analysed as a penalty method with an unknown penalty stiffness. If the real contact stiffness is too high, the HiL test will become unstable. It is therefore desirable to have control of the interaction stiffness value. For that purpose, a virtual intermediate mass m_{i} is defined, receiving the measured contact force, and interacting with the contact wire through a virtual spring with stiffness k_i as depicted in Figure 2. A controlled interaction stiffness value improves the stability of the HiL test and is the main reason for including this additional degree of freedom in the model. As shown in Section 2.4, the influence of the interaction mass is analysed and it is concluded that it has a negligible effect on the filtered contact force.

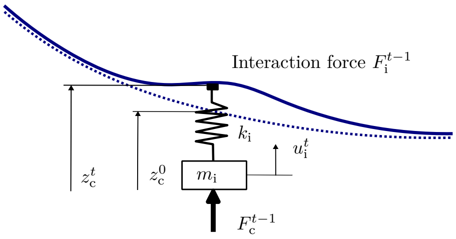

Figure 2: Interaction of a virtual interaction mass with the contact wire.

The virtual mass is a second-order system whose displacement u_i responds to the following equation:

$$m_\mathrm{i}\ddot{u}_\mathrm{i} + c_\mathrm{i}\dot{u}_\mathrm{i} + k_\mathrm{i}u_\mathrm{i} = k_\mathrm{i}z_\mathrm{c} + F_\mathrm{c} \tag{11}$$

where z_c and F_c are the reference position of the spring (the contact point height) and the external contact force from the pantograph, respectively. c_i is the damping of this subsystem.

For each time step t, the interaction between the virtual mass and the catenary is computed in several steps. First, the position of the catenary that will be sent to the actuator z_c^t is computed by solving Eq. (4), in which the force F_c^{t-1} is replaced by the interaction force F_i^{t-1} (as shown in Figure 2) and using Eq. (7).

The position of the interaction mass u_i^t is then obtained by solving Eq. (11), using the computed catenary position z_c^t and the measured contact force F_c^{t-1}. Given this position, the interaction force can be obtained as:

$$F_\mathrm{i}^t = k_\mathrm{i}\left(z_\mathrm{c}^t - u_\mathrm{i}^t\right) \tag{12}$$

2.4. Validation of the catenary

The proposed model runs in real time every time step in a PC Intel® Core™ i9-9900K CPU, 3.6 GHz, 64 GB RAM. There are however some features of the model that affect the contact force, such as the interaction mass and the explicit consideration of the contact force. In order to assess the model, the simulation results have been compared with PACDIN [19], a finite element code validated according to EN50318 [15]. Several catenary configurations and vehicle velocities have been tested, leading to the same conclusions as the results presented here. Figure 1 shows the section of a stitched catenary based on the Spanish AVE, which contains 16 equal internal spans of $L = 65$ m and 7 droppers per span. There are two transition spans at the beginning and end of the section, with different dropper distributions. The complete data of the catenary are provided in Appendix B.

d.o.f.	m (kg)	c (Ns/m)	k (N/m)
1	6.6	0	7000
2	5.8	0	14100
3	5.8	70	80

Table 1: Lumped parameters of the pantograph model for the SW catenary.

The catenary interacts with a lumped mass model of the DSA-380 pantograph (see parameters in Table 1). The simulation starts with the pantograph at the beginning of the third span. Figure 3 compares the contact force obtained from both the real-time model and the validated software, in the ten central spans. The graphs show good agreement of the forces for both the 20 Hz filtered and non-filtered data. An error index has been defined as the standard deviation of the difference, i.e. the square root of the sum of squared difference divided by the number of points, N_p:

$$\epsilon = \frac{\sqrt{\sum_{i=1}^{N_p}\left(F^i\right)^2 - \left(F^i_{\mathrm{ref}}\right)^2}}{N_p} \tag{13}$$

m_i (kg)	c_i (Ns/m)	k_i (N/m)
0.05	50	50000
m_m (kg)	c_m (Ns/m)	k_m (N/m)
10	1800	450000
m_p (kg)	c_p (Ns/m)	k_p (N/m)
5.3	10	240000

Table 2: Parameters of the virtual interaction mass, motor model and pantograph model for observer.

The parameters of the virtual mass are heuristically defined to have good agreement between the reference solution and the real-time model (see 2). An error index of $\epsilon = 7\,\%$ with respect to the mean force is obtained for the filtered contact force, and $\epsilon = 20\,\%$ for the non-filtered with good agreement in the frequency content up to 20 Hz. The interaction mass of the real-time model acts as a physical filter of the contact force, attenuating the frequencies above 20 Hz.

3. Components of the HiL test rig

Figure 4 shows a scheme of the HiL components and workflow. A linear electric motor imposes the vertical displacement computed by the virtual catenary. The motor interacts with the pantograph strip bands through contact pads containing a load cell that measures the contact force. A more detailed description of the test rig components can be found in [21].

The NI-cRIO, on the left hand side, is the real-time controller that manages all communication with the other

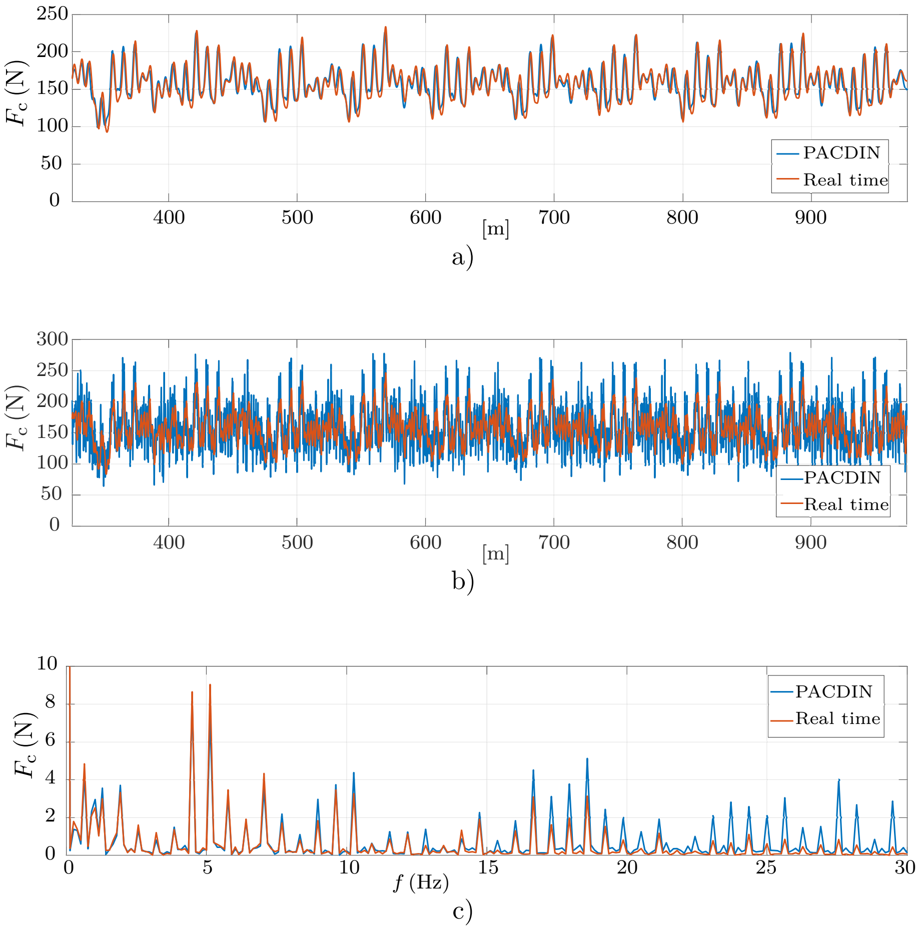

Figure 3: Comparison of the real-time model and PACDIN software contact force in the 10 central spans. a) 20 Hz filtered force, b) non-filtered force and c) non-filtered frequency content.

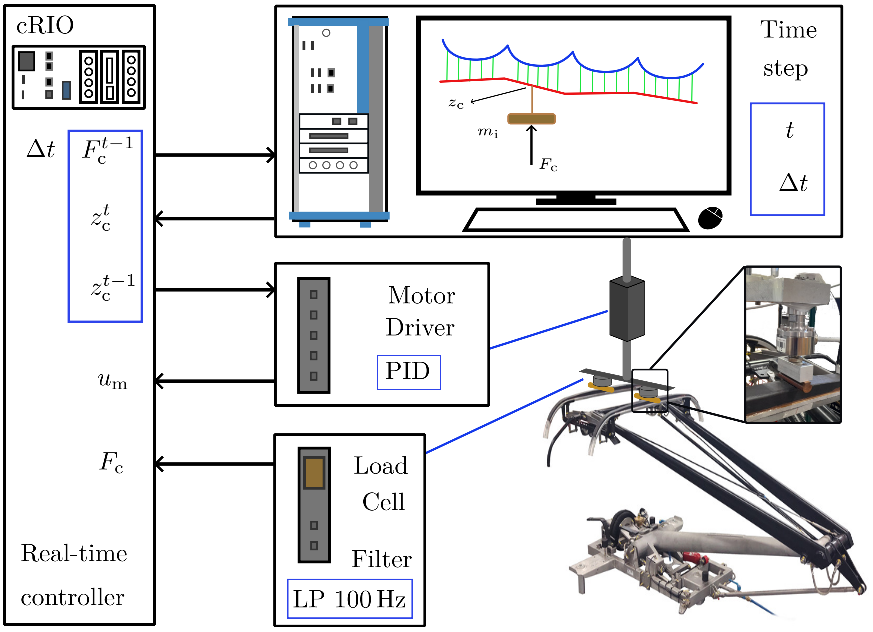

Figure 4: Scheme of the Hardware-in-the-Loop components and workflow.

components through an EtherCat real-time bus. The blue squares represent a synchronised timed loop with $\Delta t = 2$ ms controlled by the real-time cRIO. At the beginning of each loop, the contact force F_c^{t-1} and the current time step t are sent via the EtherCat bus from the cRIO to the catenary PC. The PC runs the catenary model, including the interaction mass. It must compute the new catenary position z_c^t in less than one time step, and send it back to the cRIO before the end of the timed loop. Additionally, at the beginning of the loop, the catenary position from the previous time step z_c^{t-1} is sent to the motor driver. There are two pure delays of 2 ms in the test rig workflow due to communication: the contact force used at time step t was measured in step $t-1$, and the position reference sent was computed in the previous time step.

The motor driver also provides the current position of the linear motor u_m to the EtherCat bus. The load cells' measurement of the contact forces on the pantograph strips are also available on the bus. These variables are updated at a higher rate than the timed loop. Analog-to-digital converter filters the acquired force through a 100 Hz low-pass filter.

The motor driver commands the linear motor with an internal PID with tuneable parameters. It is assumed that the actuator can be modelled as a second-order system over the bandwidth of interest, and is used to design the LQG controller. The model was experimentally identified from the step response and the parameters are shown in Table 2. The steady state value of the output is 1, the peak time is 12 ms and the peak value 1.3. The settle time is 40 ms. The transfer function of the motor response u_m with respect to the motor reference z_m can be written in the Laplace domain as:

$$G_\mathrm{m}(s) = \frac{u_\mathrm{m}}{z_\mathrm{m}} = \frac{k_\mathrm{m}}{m_\mathrm{m}\, s^2 + c_\mathrm{m}\, s + k_\mathrm{m}} \tag{14}$$

4. LQG control

The HiL test components are split into two subsystems. The first one (Subsystem 1) is the virtual catenary model that receives the force from the interaction mass F_i^{t-1}, and provides the position of the contact point z_c^t solving Eq. (4) (replacing the contact force by the interaction force) as depicted in Figure 2. This subsystem is solved with an explicit integration scheme as the force comes from the previous time step. The stability of the integration scheme was analysed for different model parameters and catenary configurations. It can be concluded that for a time increment of $\Delta t = 2\,\mathrm{ms}$, the subsystem remains stable if the virtual catenary interacts with the interaction mass through a sufficiently small stiffness k_i. Conversely, a very low stiffness value restricts the accuracy of the simulation. As highlighted in Section 2.4, the contact stiffness provided in Table 2 ensures a low contact force error while preserving the stability of Subsystem 1.

On the other hand, Subsystem 2 includes the interaction mass, linear motor and pantograph (see block diagram in Figure 5). The interaction mass receives the contact force from the pantograph F_c, and the reference position from the catenary z_c, and provides the motor reference to be achieved $z_\mathrm{m} = u_\mathrm{i}$, solving Eq. (11), and considering the communication delay. This equation can be expressed in the Laplace domain as the transfer function G_i. The motor is a second- order system with the transfer function of Eq. (14) and is attached to the contact pads that interact with the pantograph. This is shown here as a transfer function G_p for illustration, although the real pantograph behaviour is more complex.

The real pantograph interacts with the force sensor through contact pads (see Figure 4). As shown in the block diagram of Subsystem 2, the measured contact force is recovered from the contact pad stiffness k_h and the position of the actuator and the pantograph contact strips as:

$$F_\mathrm{c} = k_h\,(u_\mathrm{p} - u_\mathrm{m}) \tag{15}$$

Subsytem 2 can be unstable due to delays and high contact stiffness in the contact pads k_h. As this also makes the virtual catenary simulation unstable, a controller is proposed to stabilize Subsystem 2 with the idea that, if the motor accurately tracks the reference of the interaction mass, Subsystem 2 will be stable, thereby ensuring overall system stability.

Here we use a classical [22] state-space Linear Quadratic Regulator (LQR) controller for Subsystem 2, as depicted in Figure 6. The catenary position z_c is considered as an external perturbation, and the error is the difference between the motor reference (position of the interaction mass) and the achieved motor position, $Error = u_\mathrm{i} - u_\mathrm{m}$. The LQR controller will try to reduce the error through the action u_{lqr} added to the motor reference. This action depends on the full state of Subsystem 2, therefore a linear pantograph model is required. Since the idea is to obtain a regulator that can control different pantographs, a simple second order model is proposed for the pantograph, with the following transfer function:

$$G_p(s) = \frac{u_\mathrm{p}}{u_\mathrm{m}} = \frac{k_\mathrm{p}}{m_\mathrm{p} s^2 + c_\mathrm{p} s + k_\mathrm{p}} \tag{16}$$

The parameters of the pantograph model (see Table 2) are heuristically estimated from experimental tests, the pad stiffness k_p being the parameter that most compromises stability. The mass chosen to be equivalent to that of the pantograph strips, and a small damping is chosen. In a real HiL test, differences between the real pantograph and the model can be considered as external perturbations of the system.

The LQR calculates the optimal gain matrix that simultaneously optimizes the error of the linear motor following its reference and the control action itself. The cost

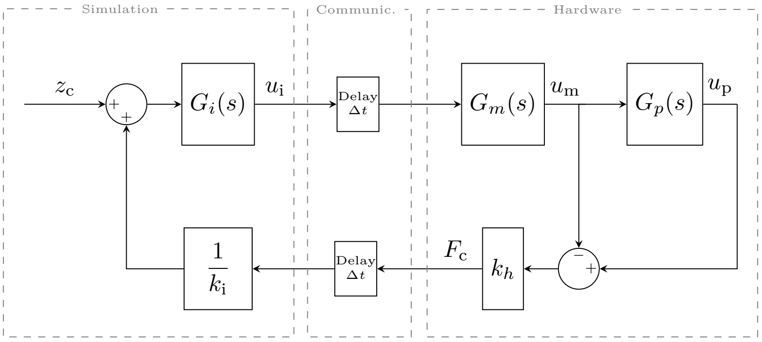

Figure 5: Block diagram of Subsystem 2: interaction mass G_i, linear motor G_m and pantograph G_p.

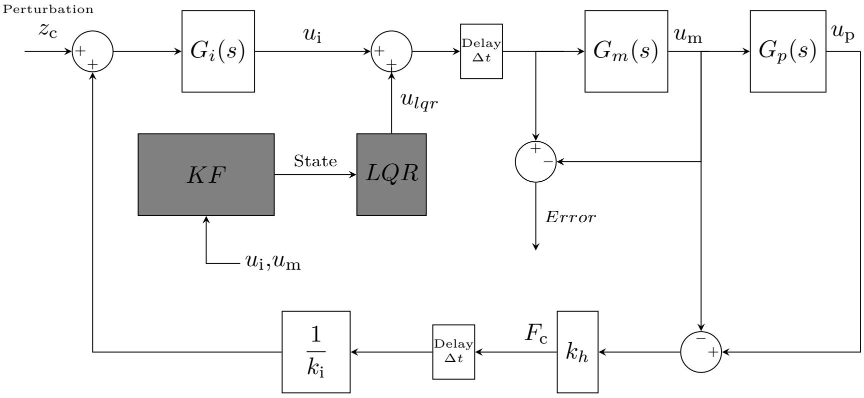

Figure 6: Block diagram of LQG controller for subsystem 2.

function can be expressed as:

$$\min_{u_{lqr}} \sum_{t=1}^{\infty} Q\left(u_{\mathrm{i}}^{t}-u_{\mathrm{m}}^{t}\right)^{2}+R\left(u_{lqr}^{t}\right)^{2} \tag{17}$$

where parameters penalizing the error Q and the action R are chosen by the user. There is a balance between a more aggressive and potentially unstable control with lower position error, if Q increases or R decreases, and a smoother control with a higher position error in the opposite tuning. The parameters used in the experimental tests are shown in Table 3 and are finely tuned heuristically. They depend on the physical characteristics of the test rig, such as the linear motor's internal controller, the friction of the linear guides, the total moving mass, and the stiffness of the contact pad. In our test rig, there is a range in which the controller stabilizes the system. If Q is increased, the position error is penalized more, and the controller attempts to increase its action and frequency content to reduce the error. Due to the practical limited bandwidth of the linear motor and the high frequencies excited in the test bench, the system may become unstable. On the other hand, if Q is reduced, the controller allows for a higher position error, causing a delay in the pantograph position relative to the catenary. An excessive delay may cause the catenary response to become unstable.

The optimal gain of the LQR depends on the full state, which is not available to the controller. A Kalman Filter [22, 23] is used as the state observer to obtain the state from measurements of the interaction mass and motor positions. The parameters tuning the KF design are given in the following subsection.

R	Q	R_{kf}	Q_{kf}
1	5	10^{-3}	10

Table 3: Parameters of the LQR controller and KF observer.

4.1. State-space equations

The discrete-time state-space model of the LQG controller and the KF observer are obtained by applying the Newmark integration scheme to the system depicted in Figure 6. The same procedure used in Section 2.1 is followed to derive the state-space model of the catenary linear part (Eq. (5) and Appendix A).

From Eq. (11) the state of the interaction mass at time $t+1$ can be written as a function of the previous state, matrix $\mathbf{A}_{\mathrm{i}}$ and vector $\mathbf{B}_{\mathrm{i}}$, and the inputs of the system. Inputs are the catenary contact point position, which is considered as a perturbation of the system, and the contact force that has a delay of one time step:

$$\mathbf{x}_{\rm i}^{t+1} = \mathbf{A}_{\rm i}\,\mathbf{x}_{\rm i}^{t} + \mathbf{B}_{\rm i}\,z_{\rm c}^{t+1} + \frac{1}{k_{\rm i}}\mathbf{B}_{\rm i}\,F_{\rm c}^{t} \tag{18}$$

where the state vector of the interaction mass is:

$$\mathbf{x}_{\rm i} = (\, u_{\rm i}\ \dot{u}_{\rm i}\ \ddot{u}_{\rm i}\,)^{\rm T} \tag{19}$$

The linear motor state-space equation can be obtained from the transfer function, Eq. (14), by again using the same Newmark integration scheme. The inputs of this system are the position of the interaction mass $u_{\rm i}$ and the control action z_m, which are delayed by one time step.

$$\mathbf{x}_{\rm m}^{t+1} = \mathbf{A}_{\rm m}\,\mathbf{x}_{\rm m}^{t} + \mathbf{B}_{\rm m}\,\mathbf{I}_u\,\mathbf{x}_{\rm i}^{t} + \mathbf{B}_{\rm m}\,z_m^{t} \tag{20}$$

where z_m^t is the delayed LQR controller action u_{lqr}, which is updated every time step

$$z_m^{t+1} = u_{lqr}^{t+1} \tag{21}$$

the state vector of the motor is defined as:

$$\mathbf{x}_{\rm m} = (\, u_{\rm m}\ \dot{u}_{\rm m}\ \ddot{u}_{\rm m}\,)^{\rm T} \tag{22}$$

and the vector $\mathbf{I}_u$ extracts the first component of the intermediate mass state, i.e. its displacement

$$\mathbf{I}_u = (\,1\ 0\ 0\,) \tag{23}$$

In the internal model, the pantograph response depends on the position of the linear motor, while the state-space equation is derived from Eq. (16)

$$\mathbf{x}_{\rm p}^{t+1} = \mathbf{A}_{\rm p}\,\mathbf{x}_{\rm p}^{t} + \mathbf{B}_{\rm p}\,\mathbf{I}_u\,\mathbf{x}_{\rm m}^{t+1} + \frac{1}{k_h}\mathbf{B}_{\rm p}\,f_{\rm p}^{t+1} \tag{24}$$

where an additional perturbation force $f_{\rm p}$ is added to consider unmodelled dynamics of the pantograph. This perturbation is used in the KF design. The state vector of the pantograph is:

$$\mathbf{x}_{\rm p} = [\, u_{\rm p}\ \dot{u}_{\rm p}\ \ddot{u}_{\rm p}\,]^{\rm T} \tag{25}$$

The last term to complete the state-space equation is the contact force, defined in Eq. (15). Using this definition in Eq. (18), and substituting Eq. (20) in Eq. (24), the following system is obtained:

$$\mathbf{x}^{t+1} = \mathbf{A}\,\mathbf{x}^{t} + \mathbf{B}_{\rm z}\,z_{\rm c}^{t+1} + \mathbf{B}_{\rm u}\,u_{lqr}^{t+1} + \mathbf{B}_{\rm f}\,Q_{kf}\,f_{\rm p}^{t+1} \tag{26}$$

where $\mathbf{A}$, $\mathbf{B}_{\rm z}$, $\mathbf{B}_{\rm u}$ and $\mathbf{B}_{\rm f}$ are defined in the Appendix C. Q_{kf} is used in the KF design and the global state vector is:

$$\mathbf{x} = \left[\mathbf{x}_{\rm i}^{\rm T}\ \mathbf{x}_{\rm m}^{\rm T}\ \mathbf{x}_{\rm p}^{\rm T}\ z_m\right]^{\rm T} \tag{27}$$

The observed variables of the system are the positions of the interaction mass and the motor:

$$\begin{aligned} \mathbf{y}^t &= \mathbf{C}\,\mathbf{x}^t + \mathbf{I}\,R_{kf}\,w \qquad \text{with} \\ \mathbf{y}^t &= \begin{bmatrix} u_{\rm i}^t \\ u_{\rm m}^t \end{bmatrix} \\ \mathbf{C} &= \begin{bmatrix} 1 & 0 & 0 & 0 & 0 & 0 & 0 & 0 & 0 & 0 \\ 0 & 0 & 0 & 1 & 0 & 0 & 0 & 0 & 0 & 0 \end{bmatrix} \end{aligned} \tag{28}$$

where w is the measurement noise, which is assumed to be equal for both measured variables, $\mathbf{I}$ is the 2x1 identity vector and R_{kf} the variance of the noise. Parameters Q_{kf} and R_{kf} are shown in Table 3.

5. Experimental results

The LQG controller is implemented in the test rig depicted in Figure 4, in the same PC containing the virtual catenary model. The dimension of the controller and observer matrices are of the order of Subsystem 2 plus the delays and can be solved with low computational cost.

A DSA-380 Steinmann pantograph is tested with the virtual catenary model described in Section 2.4. The test starts at the beginning of the 3rd span, and runs until the 16th span. Figure 7 shows the contact force in the 10 central catenary spans for a simulation at $V = 300\,\text{km/h}$. In Figure 8 the filtered contact force in the 10 central spans is depicted for train speeds of $V = 275\,\text{km/h}$ and $V = 250\,\text{km/h}$.

5.1. Validation of experimental setup

To assess the HiL test contact force $F_{\rm c}^{HiL}$ (shown in Figure 7), it should be compared with the real solution of the problem, i.e. the real tested pantograph interacting with the catenary without neither the interaction mass nor the controller. This exact solution can be iteratively obtained as follows. The HiL test contact force $F_{\rm c}^{HiL}$ is applied offline to the catenary numerical model in the simulation software PACDIN, without any pantograph model as an external given force. The simulation provides the position of the contact wire $z_{\rm c}^{Iter}$ for the full section and all time steps. This profile is applied to the linear motor in contact with the real pantograph strips without force feedback, and the contact force, $F_{\rm c}^{Iter}$, is recorded. The iterative method is schematically shown in Figure 9. This process is carried out until convergence of the contact force and the converged value is taken as reference for comparison. In practice, the changes in the contact force in every iteration are small and convergence is achieved in about 3-5 iterations. Figure 10 compares the contact force in time and frequency domains. Good agreement can be seen until 20 Hz, with an error index lower than 6 %. The results in Figure 10 can be compared to Figure 3, which shows simulation results using a lumped mass pantograph model. Even though the range of variation of the contact force is similar in the time domain, the frequency content is different. This test could be used to assess the validity of pantograph model.

Figure 11 compares the reference position of the interaction mass sent to the motor by the real-time model and the actual position attained. It can be seen that although the reference position has a higher frequency content than the motor position, the actuator is able to follow its reference with an error of less than 1 mm every time step.

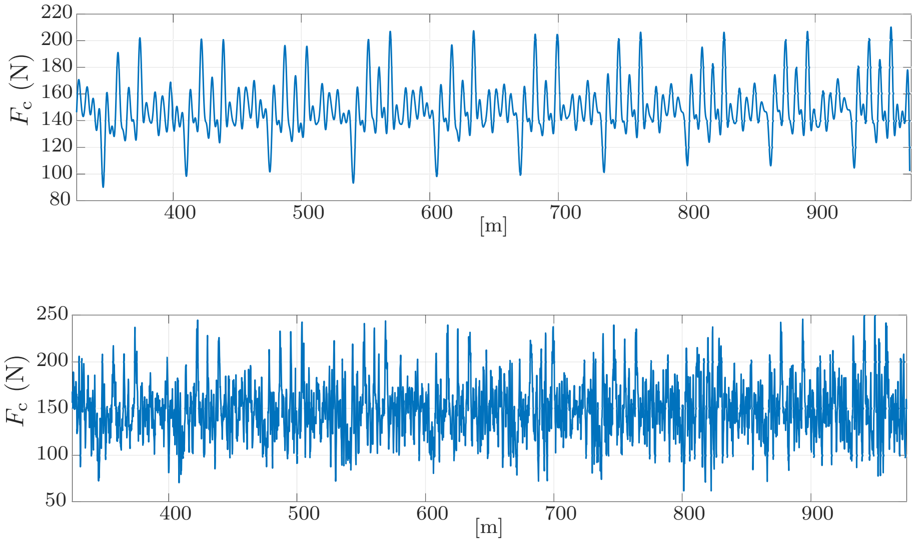

Figure 7: 20 Hz filtered and non-filtered contact force in the 10 central spans of the catenary at V=300 km/h.

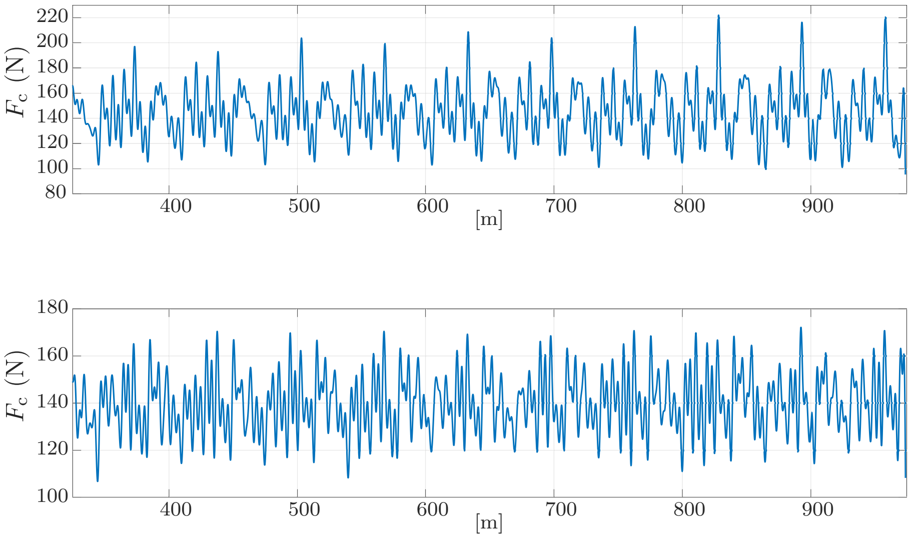

Figure 8: 20 Hz filtered contact force in the 10 central spans of the catenary at $V = 275$ km/h and $V = 250$ km/h .

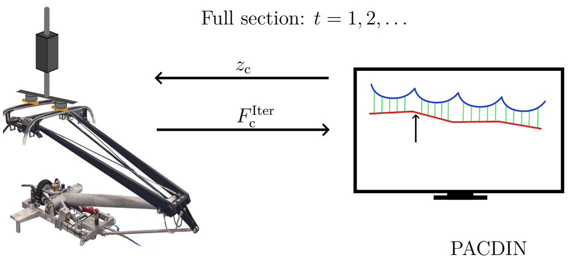

Figure 9: Iterative HiL test. The position computed for a full section is imposed in the test rig, and the experimental force is used to run a new simulation to obtain the next position.

6. Conclusions

The paper proposes a method for HiL testing of railway pantographs. The catenary model is based on modal decomposition and can handle dropper slackening. The proposed methodology can model any catenary section configuration, including presag, geometry optimization, installation errores, etc. It can run in real time for a time step of $\Delta t = 2\,\mathrm{ms}$. Despite the modal decomposition and introduction of an interaction mass between the pantograph and catenary, the model's performance is good up to a frequency of 20 Hz, with good agreement between the model and a validated code in the filtered contact force.

The interaction mass allows decoupling the real-time catenary model from other components in the test rig. The interaction of the catenary with the interaction mass

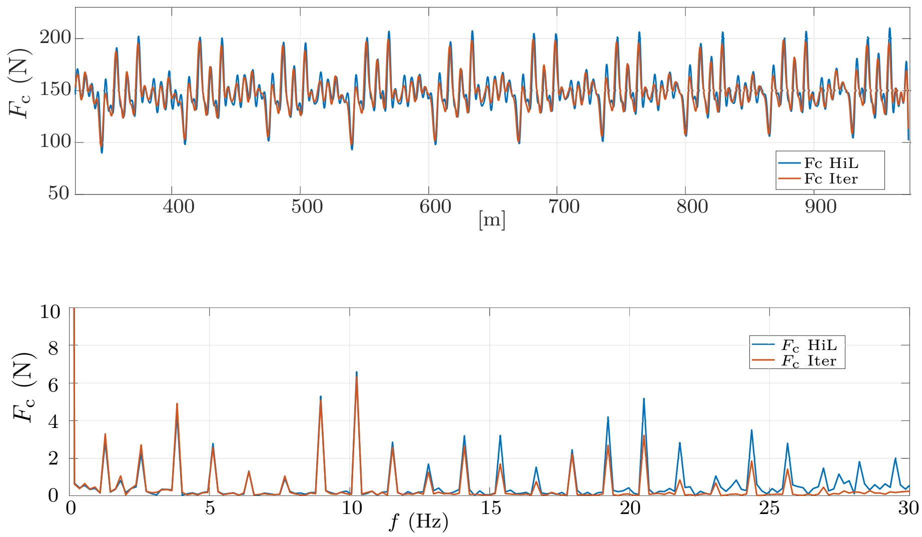

Figure 10: Comparison of filtered contact force of HiL test and reference in the 10 central spans of the catenary at V=300 km/h.

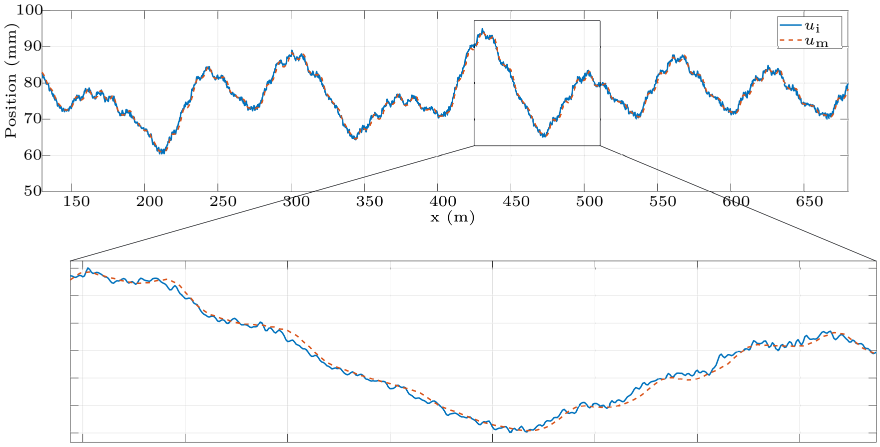

Figure 11: Comparison of the reference and achieved position of the linear motor in the 10 central spans of the catenary at V=300 km/h.

makes this subsystem stable, for the given mass, stiffness and damping. These parameters are tuned to obtain a good balance between stability and accuracy at higher frequencies.

The motor imposes the reference position on the pantograph with communication delays that can make the system unstable. An LQG controller is introduced to stabilize the system. The controller parameters are first chosen through simulation of the system, and then are finely tuned heuristically. The results show a good performance of the HiL test in the frequency range of 0-20 Hz.

Appendix A. Time integration parameters

The Newmark time integration scheme [24] is used to solve Eq. (1). It depends on two defined parameters and the time increment Δt. In this work the middle point rule (averaged constant acceleration) is used, namely $\gamma = 0.5$ and $\beta = 0.25$. The time increment is chosen $\Delta t = 2$ ms. Matrices used in Eq. (3) are defined as:

$$\begin{aligned} \mathbf{m_U} &= c_{UM}\mathbf{M}_\mathrm{c} + c_{UC}\mathbf{C}_\mathrm{c} \\ \mathbf{m_V} &= c_{VM}\mathbf{M}_\mathrm{c} + c_{VC}\mathbf{C}_\mathrm{c} \\ \mathbf{m_A} &= c_{AM}\mathbf{M}_\mathrm{c} + c_{AC}\mathbf{C}_\mathrm{c} \\ \mathbf{K_{it}}_\mathrm{c} &= c_M\mathbf{M}_\mathrm{c} + c_C\mathbf{C}_\mathrm{c} + \mathbf{K}_\mathrm{c} \end{aligned} \tag{A.1}$$

where the constants are defined as:

$$c_{UM} = \frac{1}{\beta\Delta t^2} \quad c_{VM} = \frac{1}{\beta\Delta t} \quad c_{AM} = \frac{1-2\beta}{2\beta}$$
$$c_{UC} = \frac{\gamma}{\beta\Delta t} \quad c_{VC} = \frac{\gamma}{\beta} - 1 \quad c_{AC} = -\Delta t(1 - \frac{\gamma}{2\beta})$$
$$c_M = \frac{1}{\beta\Delta t^2} \quad c_C = \frac{\gamma}{\beta\Delta t}$$

The state matrices that give the position, velocity and acceleration at time step t from the previous step can be expressed as:

$$\mathbf{A}_\mathrm{c} = \left[\begin{matrix} {\mathbf{K_{it}}_\mathrm{c}}^{-1}\,\mathbf{m_U} & \cdots \\ c_{VU}\left({\mathbf{K_{it}}_\mathrm{c}}^{-1}\,\mathbf{m_U}-\mathbf{I}\right) & \cdots \\ c_{AU}\left({\mathbf{K_{it}}_\mathrm{c}}^{-1}\,\mathbf{m_U}-\mathbf{I}\right) & \cdots \end{matrix}\right.$$

$$\left.\begin{matrix} {\mathbf{K_{it}}_\mathrm{c}}^{-1}\,\mathbf{m_V} & {\mathbf{K_{it}}_\mathrm{c}}^{-1}\,\mathbf{m_A} \\ c_{VU}{\mathbf{K_{it}}_\mathrm{c}}^{-1}\,\mathbf{m_V}+c_{VV}\mathbf{I} & c_{VU}{\mathbf{K_{it}}_\mathrm{c}}^{-1}\,\mathbf{m_A}+c_{VA}\mathbf{I} \\ c_{AU}{\mathbf{K_{it}}_\mathrm{c}}^{-1}\,\mathbf{m_V}+c_{AV}\mathbf{I} & c_{AU}{\mathbf{K_{it}}_\mathrm{c}}^{-1}\,\mathbf{m_A}+c_{AA}\mathbf{I} \end{matrix}\right] \tag{A.2}$$

$$\mathbf{B}_\mathrm{c}^t = \begin{bmatrix} {\mathbf{K_{it}}_\mathrm{c}}^{-1}\,\widehat{\mathbf{N}}_\mathrm{c}^{t\ \mathrm{T}} \\ \mathbf{0} \\ \mathbf{0} \end{bmatrix} \tag{A.3}$$

where $\mathbf{I}$ is the identity matrix, $\mathbf{0}$ is the null matrix, and constants are defined as:

$$c_{VU} = \frac{\gamma}{\beta\Delta t} \qquad c_{VV} = 1-\frac{\gamma}{\beta} \qquad c_{VA} = \Delta t\left(1-\frac{\gamma}{2\beta}\right)$$

$$c_{AU} = \frac{1}{\beta\Delta t^2} \qquad c_{AV} = -\frac{1}{\beta\Delta t} \qquad c_{AA} = 1-\frac{1}{2\beta}$$

Appendix B. Catenary data

The dropper spacing of this catenary is depicted in Table B.4 and Table B.5 gives the material properties of the different cables that form the SW catenary.

The geometric input parameters needed to define the SW catenary model are shown in Table B.6.

Appendix C. State-space matrices

The matrices in Eq. (26) are defined as follows:

$$\mathbf{A} = \begin{bmatrix} \mathbf{A}_\mathrm{i} & -\frac{k_h}{k_\mathrm{i}}\mathbf{B}_\mathrm{i}\mathbf{I}_u & \frac{k_h}{k_\mathrm{i}}\mathbf{B}_\mathrm{i}\mathbf{I}_u & \mathbf{0} \\ \mathbf{B}_\mathrm{m}\mathbf{I}_u & \mathbf{A}_\mathrm{m} & \mathbf{0} & \mathbf{B}_\mathrm{m} \\ \mathbf{B}_\mathrm{p}\mathbf{I}_u\mathbf{B}_\mathrm{m}\mathbf{I}_u & \mathbf{B}_\mathrm{p}\mathbf{I}_u\mathbf{A}_\mathrm{m} & \mathbf{A}_\mathrm{p} & \mathbf{B}_\mathrm{p}\mathbf{I}_u\mathbf{B}_\mathrm{m} \\ 0 & 0 & 0 & 0 \end{bmatrix} \tag{C.1}$$

$$\mathbf{B}_\mathrm{z} = \begin{bmatrix} \mathbf{B}_\mathrm{i} \\ \mathbf{0} \\ \mathbf{0} \\ 0 \end{bmatrix} \qquad \mathbf{B}_\mathrm{u} = \begin{bmatrix} \mathbf{0} \\ \mathbf{0} \\ \mathbf{0} \\ 1 \end{bmatrix} \qquad \mathbf{B}_\mathrm{f} = \begin{bmatrix} \mathbf{0} \\ \mathbf{0} \\ \frac{1}{k_h}\mathbf{B}_\mathrm{p} \\ 0 \end{bmatrix} \tag{C.2}$$

Acknowledgements

The authors wish to express their gratitude for the financial support received from Grant PID2020-113458RB-I00 funded by MCIN/AEI/10.13039/501100011033 and Valencian Regional Government (PROMETEO/2021/046).

References

[1] F. Mihalic, M. Truntic, A. Hren, Hardware-in-the-loop simulations: A historical overview of engineering challenge, Electronics 11 (15) (2022) 1–34. `doi:10.3390/electronics11152462`.

[2] M. Rosti, S. Cii, A. Bussini, P. Calvi, F. Ripamonti, Design and validation of a hardware-in-the-loop test bench for evaluating the performance of an active mass damper, Journal of Vibration and Control 29 (17–18) (2023) 4093–4106. `doi:10.1177/10775463221111262`.

[3] A. Haas, B. Schrage, G. Menze, P. M. Sieberg, D. Schramm, Oscillation and Vibration Reduction Approaches on a HiL-Steering-Test-Bench, IEEE/ASME Transactions on Mechatronics (2023) 1–11. `doi:10.1109/TMECH.2023.3297949`.

[4] M. Bolien, P. Iravani, J. L. d. Bois, Toward robotic pseudodynamic testing for hybrid simulations of air-to-air refueling, IEEE/ASME Transactions on Mechatronics 22 (2) (2017) 1004–1013. `doi:10.1109/TMECH.2016.2644200`.

[5] S. Kobayashi, D. P. Stoten, Y. Yamashita, T. Usuda, Dynamically substructured testing of railway pantograph/catenary system, Proceedings of the Institution of Mechanical Engineers, Part F: Journal of Rail and Rapid Transit. 233 (5) (2019) 516–525. `doi:10.1177/0954409718799900`.

[6] H. Li, F. Wang, Y. Ni, Y. Wang, Z. Xu, An adaptive and robust control strategy for real-time hybrid simulation, Sensors 22 (17) (2022) 6569. `doi:10.3390/s22176569`.

[7] G. Fermandois, Application of model-based compensation methods to real-time hybrid simulation benchmark, Mechanical Systems and Signal Processing 131 (2019) 394–416. `doi:10.1016/j.ymssp.2019.05.041`.

[8] C. Qi, D. Li, W. Ma, Q. Wei, W. Zhang, W. Wang, Y. Hu, F. Gao, Distributed delay compensation for a hybrid simulation system of space manipulator capture, IEEE/ASME Transactions on Mechatronics 27 (4) (2022) 2367–2378. `doi:10.1109/TMECH.2021.3101451`.

[9] W. Zhang, G. Mei, X. Wu, Z. Shen, Hybrid simulation of dynamics for the pantograph-catenary system, Vehicle System Dynamics 381 (6) (2002) 393–414.

[10] A. Facchinetti, S. Bruni, Hardware-in-the-loop hybrid simulation of pantograph–catenary interaction, Journal of Sound and Vibration 331 (1–12) (2012) 2783–2797.

[11] A. Schirrer, G. Aschauer, E. Talic, M. Kozek, S. Jakubek, Catenary emulation for hardware-in-the-loop pantograph testing with a model predictive energy-conserving control algorithm, Mechatronics 41 (2017) 17 – 28.

[12] S. Kobayashi, Y. Yamashita, T. Usuda, D. Stoten, Hybrid simulation testing of a pantograph-catenary system using a dynamically substructured system framework and a MDOF catenary model, Quarterly Report of RTRI 61 (2020) 127–132. `doi:10.2219/rtriqr.61.2_127`.

[13] J. Gil, M. Tur, A. Correcher, S. Gregori, A. Pedrosa, F. J. Fuenmayor, Hardware-in-the-loop pantograph tests using analytical catenary models, Vehicle System Dynamics (2021) 1–15. `doi:10.1080/00423114.2021.1962538`.

[14] J. Gil, M. Tur, S. Gregori, A. Correcher, A. M. Pedrosa, F. J. Fuenmayor, Hardware-in-the-Loop simulations of a railway pantograph with a finite element periodic catenary model, Vehicle System Dynamics (2023) 1–24. `doi:10.1080/00423114.2023.2190031`.

[15] EN 50318:2018, Railway applications. Current collection systems. Validation of simulation of the dynamic interaction between pantograph and overhead contact line, European Union Agency for Railways (2018).

[16] S. Gregori, M. Tur, E. Nadal, J. Aguado, F. J. Fuenmayor, Chinesta, Fast simulation of the pantograph–catenary dynamic interaction, Finite Elements in Analysis and Design 129 (2017) 1–13. `doi:j.finel.2017.01.007`.

[17] S. Gregori, M. Tur, A. Pedrosa, J. Tarancon, F. Fuenmayor, A modal coordinate catenary model for the real-time simulation of the pantograph-catenary dynamic interaction, Finite Elements in analysis and Design 162 (2019) 1–12. `doi:10.1016/j.finel.2019.05.001`.

	1	2	3	4	5	6	7
Longitudinal position of droppers (m)	6	15.48	24.18	32.5	40.82	49.52	59

Table B.4: Dropper spacing along the span.

	Mass/unit length (kg/m)	Axial stiffness EA (MN)	Bending stiffness EI(Nm^2)	Tension (kN)
Messenger wire	0.864	1.042	136.09	15.75
Contact wire	1.374	1.65	238.70	31.5
Stitch wire	0.091	0.11	–	3.5
Droppers	0.091	0.11	–	–
Steady arm	1	1.1	–	–

Table B.5: Material properties of the SW catenary components.

Input parameter	Value
Span length	65 m
Pre-sag	0 m
Encumbrance	1.3 m
Messenger wire stagger	0 m
Messenger wire clamp	0.2125 kg
Stitch wire length	18 m
Contact wire stagger	0 m
Contact wire clamp	0.2125 kg
Steady arm length	1.15 m

Table B.6: Geometric data of the SW catenary model.

[18] M. Tur, E. García, L. Baeza, F. J. Fuenmayor, A 3D absolute nodal coordinate finite element model to compute the initial configuration of a railway catenary, Engineering Structures 71 (2014) 234–243. `doi:10.1016/j.engstruct.2014.04.015`.

[19] M. Tur, L. Baeza, F. J. Fuenmayor, E. García, PACDIN statement of methods, Vehicle System Dynamics 53 (3) (2015) 402–411. `doi:10.1080/00423114.2014.963126`.

[20] S. Bruni, J. Ambrosio, A. Carnicero, Y. H. Cho, L. Finner, M. Ikeda, S. Y. Kwon, J. P. Massat, S. Stichel, M. Tur, The results of the pantograph-catenary interaction benchmark, Vehicle System Dynamics 53 (3) (2015) 412–435. `doi:10.1080/00423114.2014.953183`.

[21] A. Correcher, C. Ricolfe-Viala, M. Tur, S. Gregori, M. Salvador-Muñoz, F. J. Fuenmayor, J. Gil, A. M. Pedrosa, Hardware-in-the-loop test bench for simulation of catenary–pantograph interaction (CPI) with linear camera measurement, Sensors 23 (1773) (2023) 1–19. `doi:10.3390/s23041773`.

[22] P. Albertos, A. Sala, Multivariable Control Systems. An Engineering Approach, Springer Science & Business Media, 2004.

[23] R. Kalman, R. Bucy, New results in linear filtering and prediction theory, Trans. ASME Journal of Basic Engineering 83 (1961) 95–108.

[24] N. M. Newmark, A method of computation for structural dynamics, Journal of the Engineering Mechanics Division 5 (3) (1959) 67–94.